JGR Space Physics

RESEARCH ARTICLE
10.1029/2021JA029769

Key Points:

- The innermost plasmapause location remains the innermost limit of the initial sudden enhancements of energetic electrons
- Sudden enhancements observed near the duskside are often found inside the in situ plasmapause but still beyond the innermost plasmapause
- Our findings fit into the understanding of the effect of large-scale electric fields on energetic electrons and the plasmasphere

Supporting Information:

Supporting Information may be found in the online version of this article.

Correspondence to:

L.-Y. Khoo,
leng.khoo@colorado.edu

Citation:

Khoo, L.-Y., Li, X., Zhao, H., Thaller, S. A., & Hogan, B. (2021). Multi-event studies of sudden energetic electron enhancements in the inner magnetosphere and its association with plasmapause positions. *Journal of Geophysical Research: Space Physics*, *126*, e2021JA029769. https://doi.org/10.1029/2021JA029769

Received 8 JUL 2021
Accepted 25 OCT 2021

Multi-Event Studies of Sudden Energetic Electron Enhancements in the Inner Magnetosphere and Its Association With Plasmapause Positions

L.-Y. Khoo[1,2], X. Li[1,2], H. Zhao[3], S. A. Thaller[2], and B. Hogan[1,2]

[1]Department of Aerospace Engineering Sciences, University of Colorado Boulder, Boulder, CO, USA, [2]Laboratory for Atmospheric and Space Physics, University of Colorado Boulder, Boulder, CO, USA, [3]Department of Physics, Auburn University, Auburn, AL, USA

Abstract Sudden enhancements of energetic electrons (tens of keV to <500 keV) at low *L*-shells have been frequently observed by Van Allen Probes. It is, however, still unclear how deep these electrons can reach and what the responsible mechanisms are. Here we seek to determine the inner boundary of initial enhancements of these energetic electrons and its link with the plasmapause location to offer a new, insightful perspective on this topic. Previous statistical studies have revealed a remarkably consistent observation that initial enhancements of energetic electrons occur mostly at higher *L*-shell than the innermost plasmapause locations (L_{pp}), though a few outlier events were also identified. In this study, we examine the identified outlier events where electron enhancements were reported inside the plasmapause (either in situ L_{pp} or simulated innermost L_{pp}). More detailed investigation indicates that the appearance of enhancements inside the in situ L_{pp} is often associated with duskside observations where the "actual" initial enhancement likely occurs somewhere else, outside the innermost plasmapause location. We thereby urge caution when using the relationship between the observed enhancement locations and the in situ L_{pp} to infer the effect of electric fields on energetic electrons. In summary, our findings suggest that the innermost L_{pp} remains the innermost limit of the initial sudden enhancements of energetic electrons. Combining with phase space density analysis, our result implies the role of a large-scale electric field that leads to sudden electron enhancements and the erosion of the plasmasphere.

1. Introduction

With the launch of Van Allen Probes in late 2012, the twin probes have provided flux measurements near the equatorial region with fine energy and temporal resolutions. Many have utilized these detailed observations to study the energy-dependent dynamics of energetic electron (tens to hundreds of keV) populations (e.g., Reeves et al., 2016; Turner et al., 2015; Zhao et al., 2017). One frequent observation is the sudden enhancements of energetic electrons to low *L*-shells, which is a significant source of the inner radiation belt (Turner et al., 2017). What contributes to such rapid transport of energetic electrons to low *L* remains obscure. While this topic is still under active investigation, the proposed mechanisms can be generalized into two major processes. One is the effect of large-scale electric fields such as convection electric fields (Califf et al., 2017; S. Liu et al., 2003; Su et al., 2016) and subauroral polarization streams (SAPS; Califf et al., 2016; Lejosne et al., 2018). The large-scale westward electric field can open drift paths and bring energetic particles deep into the inner magnetosphere. The second is the localized resonance with electric field pulses generated by interplanetary shock (e.g., Hudson et al., 1995; Li et al., 1993; Schiller et al., 2016) or by the braking of dipolarization front bundles (Sergeev et al., 1998; Turner et al., 2015).

The effect of large-scale electric fields is commonly inferred by examining the electron enhancement locations with respect to the measured plasmapause position as well as the proton enhancement locations. The plasmasphere is a cold and dense plasma region that corotates with the Earth and is influenced by electric fields, as demonstrated by Goldstein, Sandel, et al. (2005). Under adiabatic drift theory, the energetic particles are generally subjected to the ExB drift and the gradient-B/curvature drift, whereas the cold plasma is influenced by the ExB drift only (Kivelson & Russell, 1995; Roederer, 1970). Since the ExB drift is independent of particle energy and charge, the same large-scale electric field that transports energetic particles inward is also capable of eroding the plasmasphere (Califf et al., 2017; Kivelson & Russell, 1995; Thaller

et al., 2015). Additionally, the less energetic a charged particle is, the more earthward its Alfvén layer (i.e., the boundary between the open and closed trajectories of particles) is. Under this premise, the Alfvén layer of the cold plasma should be the most earthward boundary layer as compared to that of energetic electrons. Therefore, the appearance of energetic electron enhancements inside the measured plasmapause location and the lack of observations of low-L-shell enhancement of protons at the same energy are often used to argue against the role of large-scale electric fields on sudden electron enhancement events (Reeves et al., 2016; Turner et al., 2015, 2017). Lejosne et al. (2018) have recently provided a viable explanation for the absence of the same-energy protons at low L-shells by examining the distinct influence of SAPS on different charged populations. They proposed that SAPS can transport energetic electrons inward while moving energetic ions outward. Their study, however, did not explain how sudden enhancements of energetic electrons occur within in situ plasmapause locations.

The plasmapause location is also related to different favorable growth locations for various waves. For instance, efficient acceleration mechanisms for energetic electrons like chorus waves and ultra-low-frequency waves are generally found outside of the dense plasmasphere (e.g., Thorne, 2010). Meanwhile, hiss waves that are efficient in scattering energetic electrons are predominantly found inside the plasmasphere (e.g., Malaspina et al., 2016). The energy-dependent wave-particle interaction also contributes to the formation of the prevalent bump-on-tail flux spectra inside the plasmasphere (Ni et al., 2019; Zhao et al., 2019). In short, the cold and dense plasmasphere shares an intimate relationship with energetic electrons in the inner magnetosphere (Wang et al., 2020).

Many observational studies have indeed determined an excellent association between electron enhancements, particularly relativistic electrons (>1 MeV), and the plasmapause (Foster et al., 2014; Frank, 1971; Goldstein et al., 2016; Goldstein, Kanekal, et al., 2005; Li et al., 2006). For instance, Li et al. (2006) studied long-term 2–6 MeV electron measurements from SAMPEX and identified that the initial enhancement locations of relativistic electrons are consistently found beyond the minimum plasmapause locations. The observational evidence of the dynamic linkage between tens and hundreds of keV electrons and the plasmasphere, however, is still not fully understood. Recently, Khoo et al. (2019) expanded such studies to energetic (>30 keV) electrons using Van Allen Probes data. Their work demonstrated, statistically, that the same correlation also applies to >30 keV electrons and holds regardless of the solar and/or geomagnetic conditions (Khoo et al., 2018, 2019). Nevertheless, there are also reports of enhancements found inside the in situ plasmapause locations (e.g., Turner et al., 2017) as well as a small set of events that were found inside the innermost L_{pp} (Khoo et al., 2019), which warrants a closer look at this subject. This study, therefore, seeks to investigate the cause of the observations inside the L_{pp} by examining these outlier events in depth.

The remainder of this article includes a description of energetic electron measurements and the plasmapause used in this study. Section 3 presents observations of two distinct "outlier" events in detail to examine the observed enhancement locations with respect to the in situ L_{pp} and the innermost L_{pp}, as well as a summary of all nine outlier events we examined in this study. An investigation of the phase space density evolution before and during the initial enhancement pass is presented in Section 4. The final section summarizes our findings, along with their implications on the inner magnetosphere dynamics.

2. Data and Analysis

2.1. Energetic Electron Measurements and Phase Space Density Calculation

This study uses data from Van Allen Probes (Mauk et al., 2013). The twin Van Allen Probes (also referred to as RBSP-A and RBSP-B) are identically instrumented spacecraft in the geostationary-transfer orbit with an inclination of 10° and an orbital period of ~9 h. The Magnetic Electron Ion Spectrometer (MagEIS) instrument (Blake et al., 2013) onboard Van Allen Probes offers finely resolved flux measurements for a wide range of electrons (~30 keV–~4 MeV with an energy resolution of $\Delta E/E \approx 30\%$). In this study, we employ spin-averaged measurements of 30 keV to ~2 MeV electrons from MagEIS to identify the inner boundary of the sudden enhancement events.

To complement the electron flux measurements from Van Allen Probes, we use energetic electron measurements from Geostationary Operational Environmental Satellites, GOES 13 and GOES 15, which provide information of energetic electrons at the geostationary orbit. Energetic Particle Sensor MAGnetospheric

Electron Detector onboard GOES 13 and GOES 15 supplies the electron fluxes in five channels (30–50, 50–100, 100–200, 200–350, and 350–600 keV). This study uses one-minute averaged flux measurements that were corrected for deadtime errors and other contamination sources (Hanser, 2011). There are nine MAGED telescopes pointing at different directions on the GOES spacecraft and only the data from the telescope pointing closest to the equatorial plane (i.e., perpendicular to the local magnetic field) is used in this study.

For a complete radial coverage in our phase space density analysis, we utilize flux measurements from Helium, Oxygen, Proton, and Electron Mass Spectrometer (HOPE) in addition to the MagEIS observations and we average the flux measurements for the overlapped energy channels between MagEIS and HOPE. Electron fluxes are then converted to phase space density using the method described in Chen et al. (2006). The PSD results shown in this manuscript use the T89D external magnetic field model (Tsyganenko, 1989) and IGRF internal magnetic field (Finlay et al., 2010) that were provided in the Van Allen Probes magnetic ephemeris file. Although not shown here, we also conduct the same phase space density analysis using different magnetic field models like TS04 (Tsyganenko & Sitnov, 2005) and Olson-Pfitzer quiet-time field model (OP77Q; Olson & Pfitzer, 1977) and obtain comparable results (see Figures S1–S4 in Supporting Information S1).

2.2. Plasmapause: Definition, Determination, and Simulations

This study uses two different plasmapause values (L_{pp}): measured in situ L_{pp} and simulated L_{pp} to provide a global context of the plasmasphere. The in situ L_{pp} is commonly identified from the measured plasma density gradient, which is defined as a factor of 5 drop in density within a distance of 0.5 L (Carpenter & Anderson, 1992). However, this definition is not easy to implement. As pointed out by Moldwin et al. (2002), even though the plasmapause can be identified in ~73% of the passes in their study, only ~16% of the identified plasmapause have the clean and sharp "classic" plasmapause. An alternative to this L_{pp} definition is to use a density threshold (n_e) of 100 cm^{-3} to infer the plasmapause. Many studies have utilized the density threshold as a proxy of the plasmapause position (Chappell et al., 1970; Malaspina et al., 2016; Thaller et al., 2019). In Thaller et al. (2019), they derived the plasmapause using both the plasma density gradient and density threshold methods and demonstrated that these two quantities are comparable. They further noted that the plasmapause derived from the density threshold has fewer gaps, thanks to its simplicity of implementation. The good agreement between these two approaches was explained by Malaspina et al. (2016) through their statistical study; they found that the steepest plasma density gradient often occurs near a plasma density of 100–200 (~50) cm^{-3} at $L < 4$ ($L > 4$). Therefore, this study uses the plasma density threshold of 100 cm^{-3} to determine if the enhancements happen inside ($n_e > 100$ cm^{-3}) or outside ($n_e \leq 100$ cm^{-3}) the plasmasphere.

The plasma density was derived from the spacecraft potential measurements using the electric field and waves (EFW) instrument (Escoubet et al., 1997; Wygant et al., 2013) and from upper hybrid resonance measurements using the Electric and Magnetic Field Instrument Suite and Integrated Science (EMFISIS) instrument (Kletzing et al., 2013; Kurth et al., 2015). Both approaches have their pros and cons; the former is more accessible even during geomagnetic active periods but only serves as a proxy for the plasma density, while the latter is a more robust approach, but the measurements can be difficult to interpret during geomagnetic active periods. Interested readers may refer to Jahn et al. (2020) for a more comprehensive discussion. This study presents the plasma density profiles from both instruments (EFW and EMFISIS). The plasma density measurement from EMFISIS is primarily used in the case where the plasma density measurements are available from both instruments.

In this study, we also obtain the global evolution of the plasmapause using the Plasmapause Test Particle (PTP) simulations. The plasmapause in the PTP simulation is represented as the boundary of a cold test particle ensemble (Goldstein, Sandel, et al., 2005) that is subjected to ExB drift. The simulation is driven by an empirical model of the convection electric field (Stern, 1975; Volland, 1973) and an analytical representation of SAPS. The time resolution of the PTP simulation is 15 min. Goldstein, Pascuale, et al. (2014) have previously simulated the plasmapause crossing events using the PTP simulations and obtained a good agreement (a mean uncertainty of 0.40 ± 0.05 R_E) with the observed plasmapause locations by Van Allen Probes. The simulated plasmapause location is represented in dipole L value, which is defined as the radial distance in the magnetic equator in Earth radii, R_E. In the subsequent comparison, the simulated L_{pp} is transformed to the Geocentric Solar Magnetospheric (GSM) coordinates by rotating about the y-axis for the

dipole tilt angle, which is the angle between the Earth's north dipole axis and the GSM-Z axis. The dipole tilt angle was obtained from the magnetic ephemeris file provided by the Van Allen Probes. The minimum L_{pp} in this study refers to the most earthward plasmapause location of all local times at a specific time instant, and the innermost L_{pp} generally refers to the lowest of all minimum L_{pp} between the starting time of the substorm and the time when the inner boundary of the initial enhancements of energetic electrons was identified.

3. Event Overviews

We studied nine enhancement events that were previously reported inside the in situ plasmapause locations (Turner et al., 2015, 2017) or inside the simulated innermost plasmapause locations (Khoo et al., 2019). The definition of enhancements used in this study is the same as that used in our previous studies (Khoo et al., 2018, 2019): an order of magnitude or more increase in flux between two subsequent passes of the same probes across an arbitrarily determined L range, $\Delta L \geq 1$. For the outlier events reported inside the in situ L_{pp}, we decrease the L range criteria from ≥1 to ≥0.5 to ensure we capture the enhancement events that were observed by other studies (Turner et al., 2015, 2017). The initial sudden enhancement is the earliest enhancement that was first observed between the two probes. The L values used in this study are derived using the OP77Q magnetic field model. In this section, we examine two different enhancement events in detail and present a summary of our results for all nine outlier events at the end of this section.

3.1. The October 14, 2014 Event

The October 14, 2014 event is a relatively weak geomagnetic storm with Dst > -50 nT that was driven by corotating interaction regions (CIR; Shen et al., 2017). Figure 1 shows flux measurements from the Van Allen Probes and GOES 13 and GOES 15 between October 13 and October 15, 2014. The dashed black line indicates the onset of substorms at 13 UT on October 14, 2015. The apogee of the Van Allen Probes in this event was near the post-midnight sector as shown in Figure 3. This enhancement event was previously reported inside the minimum L_{pp} that were inferred from both X. Liu et al. (2015) plasmapause and PTP simulation models (Khoo et al., 2019).

Figure 1 shows that flux enhancements of 40–150 keV electrons were first observed by both GOES 15 and GOES 13 around 14:20 UT (5.6 MLT) and 14:30 UT (9.8 MLT), respectively. The inner boundary of 30 keV electron enhancements was subsequently observed by RBSP-A a few minutes after, ~14:37 UT, at $L = 4.71$ (2.1 MLT) during its outbound pass. It is therefore likely that RBSP-A observed the same enhancement event that was measured by the GOES spacecraft earlier and is near the actual enhancement locations when it observed the initial enhancements. Note that the initial enhancements of higher energy like 54 and 120 keV electrons were also observed during this storm event, but those enhancement events were outside of the innermost plasmapause location. Therefore, there is only one outlier event during this storm period, and we only show observations for 30 keV electrons in Figure 1. The in situ plasma density measured by EMFISIS and EFW instruments onboard the Van Allen Probes are shown in Figure 1e. We determined that the inner boundary of the initial enhancement was outside the in situ plasmapause based on its plasma density, n_e ~20 cm^{-3}. Here we focus only on the initial enhancement of 32 keV electrons. However, we note that during this storm period, the initial enhancement of 346 keV electrons was also found inside the innermost L_{pp}. This particular initial enhancement event was identified approximately one day after the initial enhancements of tens of keV electrons. That is because even though significant flux enhancements were observed at an earlier pass, they did not fulfill the L range criteria ($\Delta L \geq 1$, while it has $\Delta L \sim 0.8$) for our initial enhancement definition. When we decrease our L range criteria to $\Delta L \geq 0.5$, we find that the initial enhancement of 346 keV electrons remains outside of the in situ L_{pp}, like what we observed with the initial enhancement of 32 keV electrons.

Figure 2 illustrates in detail how the flux varies between two consecutive passes for 10 keV to 2.5 MeV electrons. Particularly, Figures 2a and 2b provide the flux evolution of 10 keV to 2.5 MeV electrons measured by RBSP-A at two different L values: (a) $L = 4.26$, the in situ L_{pp} that was defined as the lowest L-shell with the plasma density closest to 100 cm^{-3}; (b) $L = 4.71$, the inner boundary of the initial enhancement for 32 keV electrons. Even though we also observe an increase in flux for 54 keV electrons in Figure 2b, the

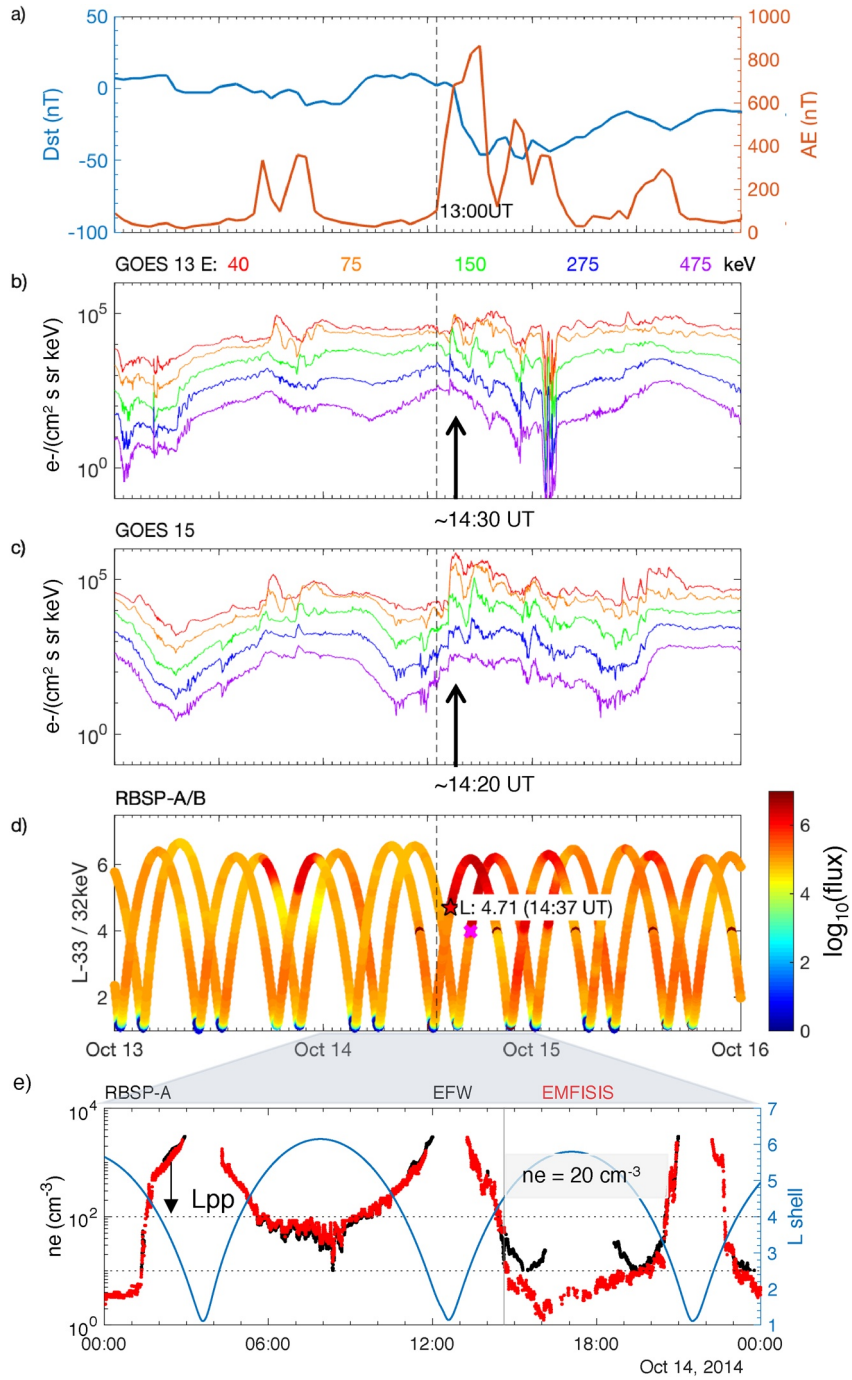

Figure 1. (a) Dst (blue) and AE (red) indices between October 13–15, 2014. The dashed black line shows the onset time of the substorm (13 UT) on October 14, 2014. (b–c) Flux variations of the five energy channels from GOES 13 and GOES 15. The median energies of each energy channel are 40 keV (red), 75 keV (orange), 150 keV (green), 275 keV (blue), and 475 keV (purple), respectively. The corresponding flux enhancement time is marked using the black arrow and listed accordingly. (d) Flux measurements of 33/32 keV energetic electrons from Van Allen Probes between October 13–15, 2014. The *y*-axis lists the plotted electron energies from RBSP-A and RBSP-B, respectively. The inner boundary of the initial enhancement is indicated by the black-edge star with the corresponding enhancement time and *L*-values listed in the inserted white box. The unit of flux is #/(cm^2 sr s keV). (e) Plasma density from RBSP-A on October 14, 2014. The red and black lines show plasma density results from EFW and EMFISIS, respectively. The highlighted vertical gray bar indicates the time when the inner boundary of the initial enhancement occurs, and the corresponding plasma density is listed in the inserted gray box. The blue line indicates the *L*-shell. Two horizontal dotted black lines highlight two plasma densities, n_e = 10 and 100 cm^{-3}.

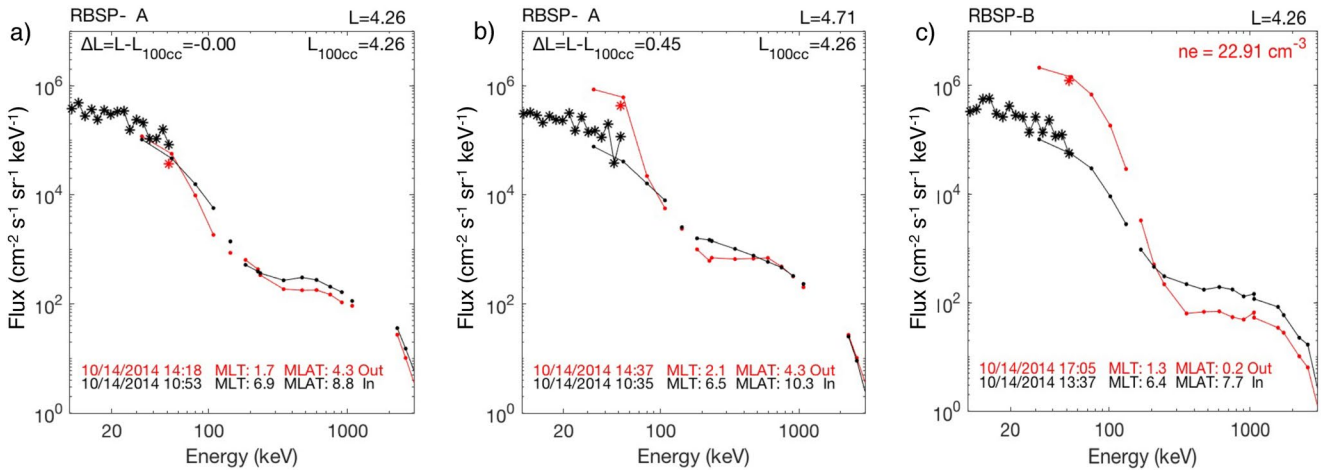

Figure 2. (a–b) Energy spectra of electrons measured by RBSP-A between two subsequent passes as indicated by the black (inbound pass) and red (outbound pass) lines. They present energy spectra at two different L values: at the in situ L_{pp} and the inner boundary of enhancements. The identified in situ L_{pp} on the outbound pass where the initial enhancement event was observed is listed on the top right of each plot and is defined as the lowest L-shell at which the plasma density is the closest to 100 cm^{-3}. The distance between the in situ L_{pp} and the corresponding L value (listed on the top right) is also presented, where the positive (negative) value indicates that the inner boundary of the initial sudden enhancement is outside (inside) the in situ L_{pp}. The data with asterisks are from the HOPE instrument and the dotted data are from the MagEIS instrument. (c) Energy spectra of electrons measured by the following RBSP-B during its inbound (black) and subsequent outbound (red) passes. The plasma density measured by RBSP-B during the outbound pass is also listed on the top right of the plot.

flux enhancement for 54 keV electrons does not sustain over a wide L range (in this case, $\Delta L < 0.5$), and therefore, we only identify sudden flux enhancements of 32 keV electrons during this outbound pass. When comparing the energy spectra evolution at and outside the in situ L_{pp} (Figures 2a and 2b, respectively), it is notable that no drastic flux variation is observed for 10 keV–2.5 MeV electrons at the in situ L_{pp}. This energy spectra evolution is also consistent with our previous report that the energy spectrum inside the innermost L_{pp} remains unchanged before and during the initial enhancement event (Khoo et al., 2018). Trailing behind RBSP-A, RBSP-B also observes at least an order of magnitude increase in fluxes at the subsequent outbound pass, but for 30–132 keV electron (Figure 2c). This supports the earlier observations by GOES that flux enhancement was observed for 40–150 keV electrons. The contrast between RBSP-A and RBSP-B energy spectra also highlights the importance of the timing and spacecraft locations in understanding energetic electron dynamics. Since the plasma density profile from RBSP-B is incomplete during this outbound pass, we only provide the plasma density at $L = 4.26$. Like RBSP-A, the plasma density measurement indicates that RBSP-B remains outside of the in situ L_{pp} during its outbound pass when it observes flux enhancements for 30–132 keV electrons.

We next examine where the initial enhancement observed by RBSP-A occurs with respect to the simulated plasmapause location in the GSM coordinates at three different timestamps: when the substorm begins (13 UT), when flux enhancements were first observed by the GOES spacecraft (~14:20 UT), and when the inner boundary of the initial sudden enhancement was observed by RBSP-A (14:37 UT). The plasmapause locations for all local times at the specific timestamp are plotted in Figure 3 as solid tangerine yellow lines. The innermost L_{pp} between the beginning of the substorms and the specific timestamp were outlined as dotted black lines. The simulated plasmapause in Figure 3 suggests that a residual plume rotates eastward and wraps around the main plasmasphere at the time when the initial enhancement was observed around 14:37 UT. The multiple layers of the plasmaspheric plume in Figure 3 indicate the wrapping of the plasmaspheric plumes during this event; this feature was previously discussed in Goldstein, Thomsen, and DeJong (2014). Due to the eastward rotation of the plasmaspheric plume, the plasmapause near the midnight sector was located at higher L values. The innermost L_{pp}, in this case, was found near the dawn sector and incidentally, RBSP-A was near the local time of the simulated innermost L_{pp} when it observed the inner boundary of the initial enhancement event. Based on the simulated plasmapause, the inner boundary of the initial enhancement was just inside the simulated innermost L_{pp}. However, the measured plasma density profile indicates otherwise, suggesting that RBSP-A was just outside of the in situ L_{pp}. This discrepancy between model and

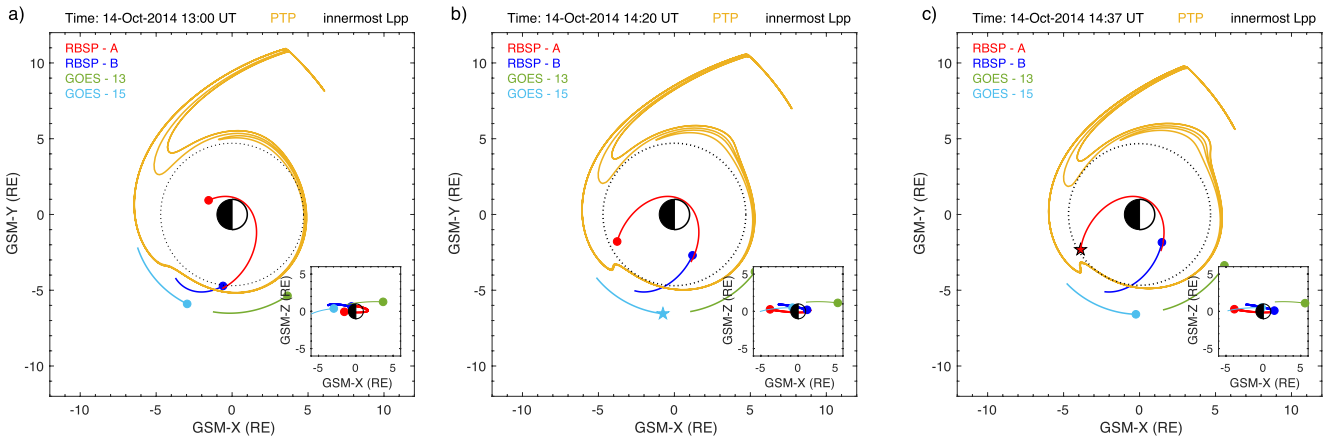

Figure 3. Location of Van Allen Probes and GOES 13 and 15 as well as the plasmapause locations from the PTP simulations at three different timestamps: (a) The onset time of the substorm (b) the time when flux enhancements were observed by the GOES spacecraft (c) the time when the inner boundary of initial enhancement was first observed by RBSP-A. Both the solid circle and the star symbol represent the location of the spacecraft at the time indicated on the top left of the plot, with the star symbol highlights the spacecraft that observes flux enhancements at the specific timestamp. The solid lines trailing the solid/star symbols show the trajectory of the spacecraft three hours prior to the specific timestamp. The dotted black lines indicate the innermost L_{pp} between the start time of the substorm to the specified timestamp. The small insert on the bottom right of each plot illustrates the spacecraft locations in GSM-Z and GSM-X coordinates.

observation is understandable since the PTP simulation (mean uncertainty of 0.4 ± 0.015) does not include quiet-time processes like neutral wind coupling (Burch et al., 2004) or interchange instability (Lemaire & Gringauz, 1998) and thus has a higher uncertainty during the recovery/quiet period, as noted by Goldstein, Pascuale, et al. (2014). Despite that, the proximity between the innermost L_{pp} and the inner boundary of the initial enhancements suggests that the innermost L_{pp} remains a good proxy of the inner boundary of the initial enhancements.

3.2. The July 25, 2013 Event

The July 25, 2013 event is considered as a non-storm event with Dst > −20 nT but is associated with substorm activity (AE_{max} = 749 nT, starting at 15 UT on July 25, 2013). Figure 4 showcases the flux enhancements of ∼33, ∼75, and ∼143 keV electrons from the Van Allen Probes since the sudden enhancements observed in this event were limited to $E \leq 145$ keV (see also Figure 5). The corresponding L-shell and the time near the observed inner boundary of the initial enhancement event (specified as black-edged red stars) are also listed. As shown in Figures 4 and 6, GOES 13 was heading toward the noon sector during the onset of the substorm and did not observe any obvious flux enhancements. GOES 15, on the other hand, only has equatorial flux measurements for >150 keV electrons during that period, and hence we can only verify the flux increase of the 150 keV electron channel around 21 UT. The apogee of the Van Allen Probes during this event was near the duskside. The inner boundary of the initial enhancement of 32–132 keV electrons was first observed by RBSP-B between 22:46 UT to 23:13 UT during its outbound pass, at L = 3.88–4.75. Based on the plasma density profile for this outbound pass, we identified the in situ L_{pp} to be L = 4.99. The comparison of the in situ L_{pp} and the inner boundary location verifies that the initial sudden enhancements for 32–132 keV electrons were within in situ plasmapause positions; thus, it is counted as one of our outlier events.

Figure 5 describes the energy spectrum evolution between the inbound and outbound passes before and during the initial enhancements of energetic electrons. As seen in Figure 5a, 75 keV electrons is the only energy channel that observed a large magnitude of flux increase at $L \sim 3.88$, which was the inner boundary of the initial sudden enhancement for this particular energy during this event and was ∼1 L inside the in situ L_{pp}. Flux enhancements over a wide range of energies from 20 to 143 keV are identified at the in situ L_{pp} (Figure 5b). We also observe a very different energy spectra evolution in Figure 5 than in Figure 2: flux enhancements were observed for different electron energies at and inside the in situ L_{pp} in Figure 5. This discrepancy suggests that sorting/comparing flux enhancements with the in situ L_{pp} is likely to yield an

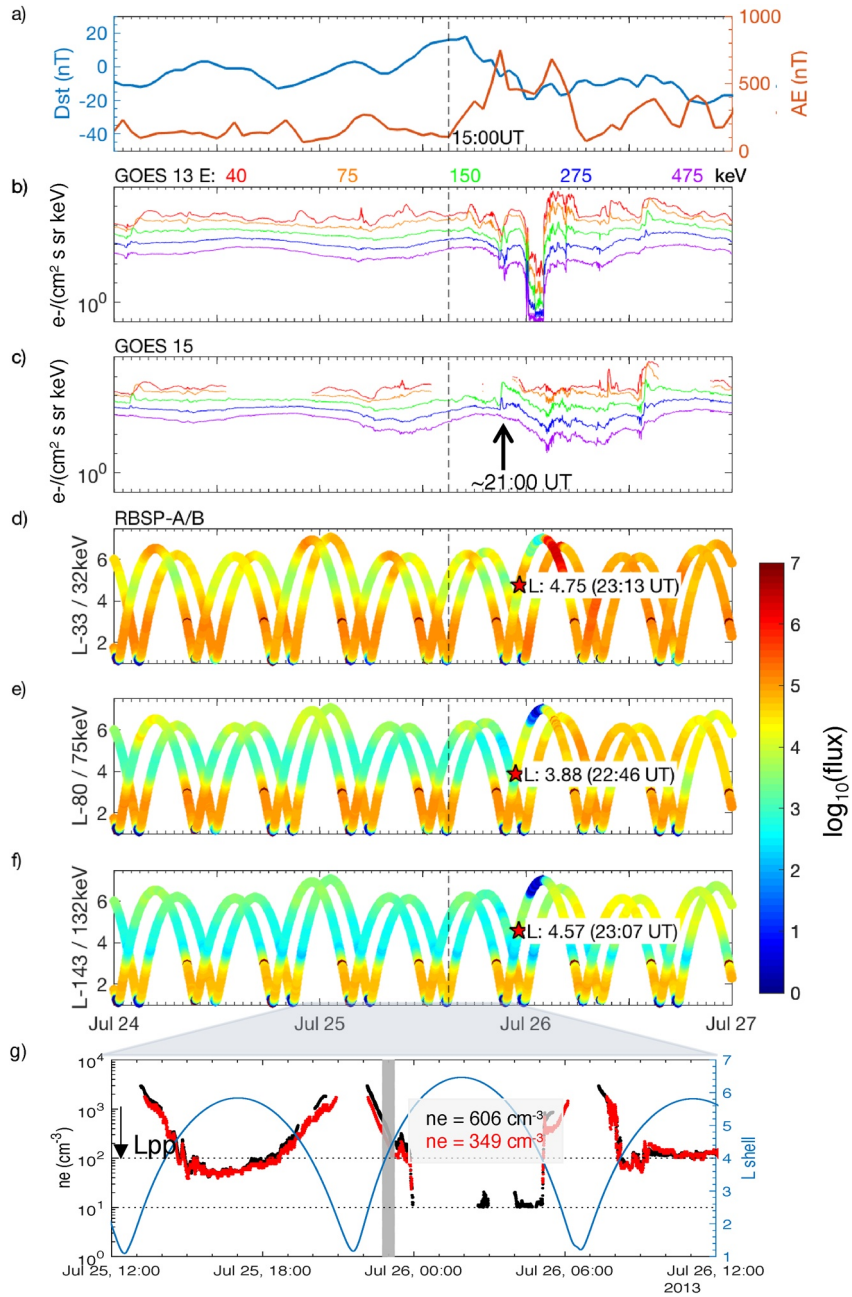

Figure 4. Like Figure 1, but for the July 25, 2013 event with the flux measurements from three different electron channels: 33/32, 80/75, and 143/132 keV for RBSP-A and RBSP-B, respectively; (g) The highlighted vertical gray bar covers the time for the inner boundary of the initial sudden enhancements of ~30–~145 keV electrons.

incoherent conclusion due to the local-time dependency of the plasmasphere and the localized nature of the spacecraft observations. In this event, the spacecraft was unfortunately located far from the local time of the actual initial enhancement and was near the dusk side when observing the initial enhancement events. For such events, the innermost L_{pp} could serve as a good proxy for the plasmapause location near the actual initial enhancement locations and thus a better estimate for the inner boundary of initial enhancements, as shown in Figure 6 and previous statistical studies (Khoo et al., 2018, 2019).

This event was also studied in depth by Turner et al. (2015) using 13 different spacecraft. Therefore, we refer to Turner et al. (2015) to provide information on energetic electrons at other locations. According to their

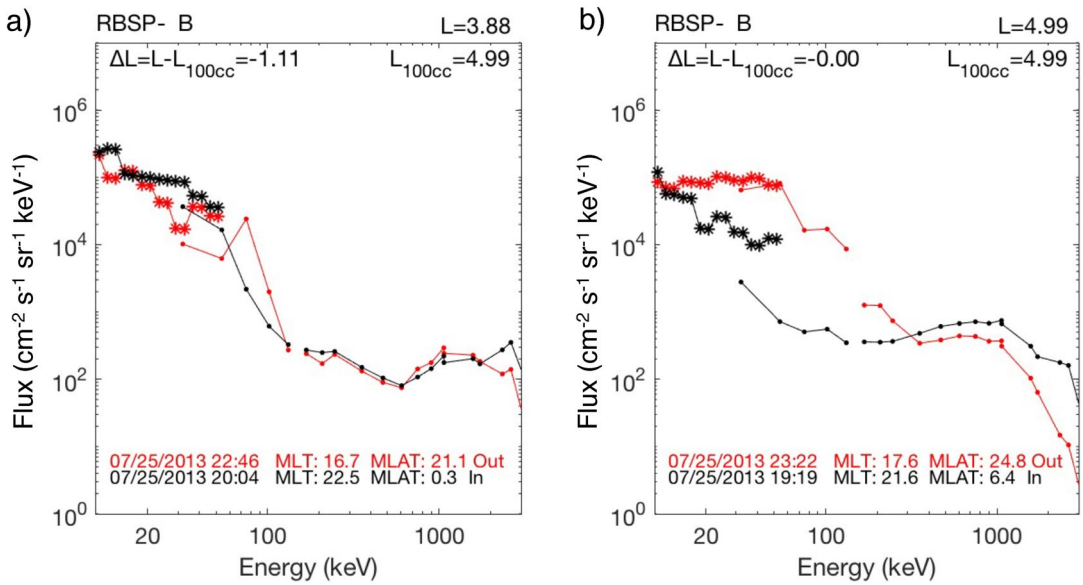

Figure 5. Same as Figure 2, but for the July 25, 2013 event.

study, two injections were observed below geosynchronous orbit during this event. The first enhancements were observed by LANL-04A and LANL-02A around 20:46 UT (~3 MLT) and 20:48 UT (~5 MLT), and the local time distance between the two spacecraft marks the local time limit of the first enhancement/injection. The second deep injection was observed first by LANL-04A at 21:25 UT. Due to the difference in our enhancement definition, we identified a slightly higher inner boundary of the initial sudden enhancement than Turner et al. (2015). We, however, have verified that in both scenarios, the initial sudden enhancements coincide or stay beyond the innermost L_{pp} (Figure 6c).

The simulated innermost L_{pp} refers to the lowest plasmapause position of all local times between 15 UT and 22:46 UT. In this case, it represents the plasmapause position near the postmidnight sector, which is consistent with the local time of the LANL-02A and LANL-04A when they observed flux enhancements. In other words, the innermost L_{pp} is likely associated with the plasmapause location near the actual enhancement region. The initial sudden enhancements were determined inside the in situ L_{pp} (near the dusk sector) but beyond the innermost L_{pp} (near the postmidnight sector), as seen in Figure 6. This result can be explained by the combined effect of ExB and gradient-B/curvature drift. Once the energetic electrons are transported to such low L, the gradient-B/curvature drift is likely to dominate and forces them to drift eastward. As

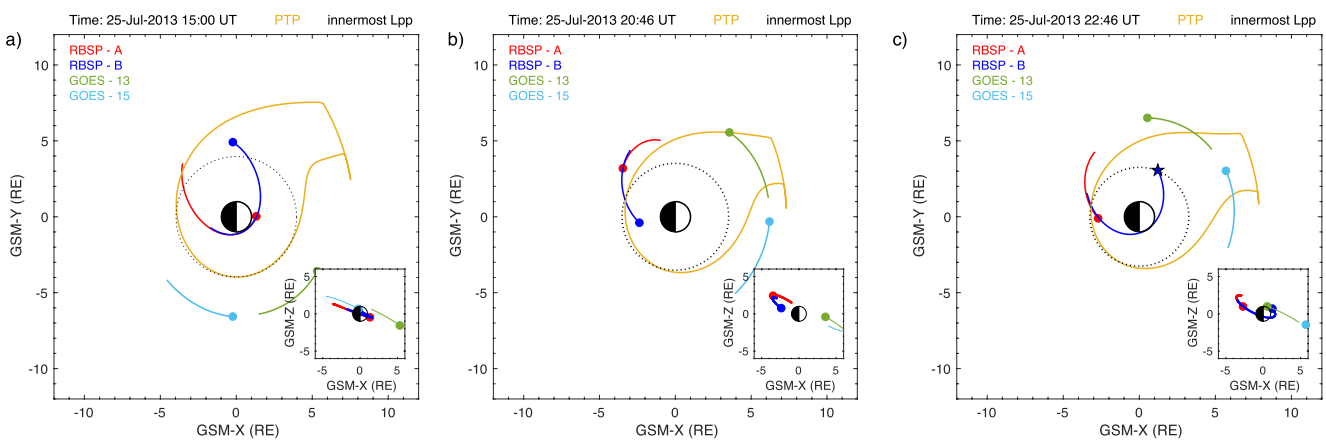

Figure 6. Like Figure 3, but for July 25, 2013 event. (b) The location of the Van Allen Probes and GOES spacecraft when flux enhancements were first observed by LANL-04A at 20:46 UT.

Table 1
Geomagnetic Indices (Dst and AE Index), the Distance Between the Inner Boundary of Initial Enhancement Events and the Simulated Innermost L_{pp} (ΔL), the Corresponding Plasma Density (n_e), the Magnetic Local Time (MLT) for the Outlier Events Examined in This Study, and the MLT of the Innermost L_{pp} During the Initial Enhancements

Event	Dst_{min} (nT)	AE_{max} (nT)	ΔL	n_e (cm^{-3})	MLT of the observed initial enhancements	MLT of the innermost L_{pp}
10/14/14	−49	864	−0.19	51.46	Post-midnight (2)	Pre-noon (8.6)
3/1/13	−55	935	0.44	161.02	Post-midnight (4.1)	Post-midnight (2.9)
11/4/14	−44	856	0.07	41.82	Post-midnight (5.8)	Pre-noon (6.4)
12/17/12	−11	589	0.09	763.59	Pre-noon (7.4)	Post-midnight (2.7)
7/23/15	−63	1,162	−0.11	841.87	Post-noon (14.6)	Pre-noon (7.0)
7/25/13	−19	749	0.12	349.14	Post-noon (16.5)	Post-midnight (2.8)
5/18/13	−61	1,009	0.55	239.64	Pre-midnight (19.8)	Post-midnight (4.7)
6/22/15	−204	1,636	−0.15	926.05	Pre-midnight (20.9)	Post-midnight (2.5)
6/8/15	−73	957	−0.43	838.81	Pre-midnight (21.7)	Post-midnight (2.8)

noted by Turner et al. (2015), the enhancements detected by Van Allen Probes are likely related to the enhancements observed first by the geosynchronous satellites. They also determined that one of the THEMIS spacecrafts, TH-A, passed through the plasmapause around 21:02 UT, at $L = 3.7$ and 05:10 MLT. Based on the PTP simulation, TH-A was likely measuring the minimum plasmapause location. Assuming a simple dipole magnetic model, a 75 keV electron at $L = 3.88$ can complete its drift in ~2.4 hr. Because of their orbit, Van Allen Probes only detect a significant flux enhancement an hour or two after at ~17 MLT (22:46 UT) and were inside the plasmaspheric bulge/plume during that time, according to the projected global plasmapause locations by the PTP simulation (Goldstein, Sandel, et al., 2005). This is thus supportive of our observations that the initial flux enhancements were observed inside in situ L_{pp} but remain outside the innermost L_{pp}. This event also demonstrates that the innermost L_{pp} is a good proxy for the plasmapause location near the actual initial enhancement event, and it is particularly useful in the case when the spacecraft is located far from the actual initial enhancement such as this event.

3.3. Summary of the Outlier Events

This section provides a summary of the relationship between the "outlier" enhancement events and the in situ plasma density as well as the innermost L_{pp}. Table 1 lists nine outlier events with the minimum Dst and maximum AE index, the distance between the innermost L_{pp} and the inner boundary of the initial enhancements (among all energy channels) during a specific event, the corresponding plasma density, the magnetic local time (MLT) of the observed initial enhancements by the Van Allen Probes as well as the MLT of the innermost L_{pp} during the initial enhancements. Note that the events in Table 1 are arranged according to the MLT of the observed initial enhancement events. The MLT are further categorized into four different sectors: post-midnight (0–6 MLT), pre-noon (6–12 MLT), post-noon (12–18 MLT), and pre-midnight (18–0 MLT). In this section, we only study the "innermost" of all the initial enhancements from different energy channels during a specific event, and these "innermost" initial enhancements are from 32 to 80 keV electrons. This is relevant to the energy-dependent dynamics of energetic electrons discussed in previous studies like Khoo et al. (2019) and Reeves et al. (2016) that enhancements of lower-energy electrons often occur earlier than higher-energy electrons.

To complement Table 1, Figure 7 presents the location of these initial enhancements for all outlier events in the GSM System coordinate. The colors in Figure 7a represent the distance of the inner boundary of initial enhancements from the innermost L_{pp}. The negative (positive) ΔL means the inner boundary is inside (outside) the innermost L_{pp}. Based on Table 1 and Figure 7a, five out of nine events were found outside of the innermost L_{pp}, while the other four events were <0.45 L inside the innermost L_{pp}. Our earlier statistical studies (Khoo et al., 2018, 2019) examined CME- and CIR-driven storms that occurred between January 2013 and June 2015 and identified 231 initial enhancement events across different electron energies. Only

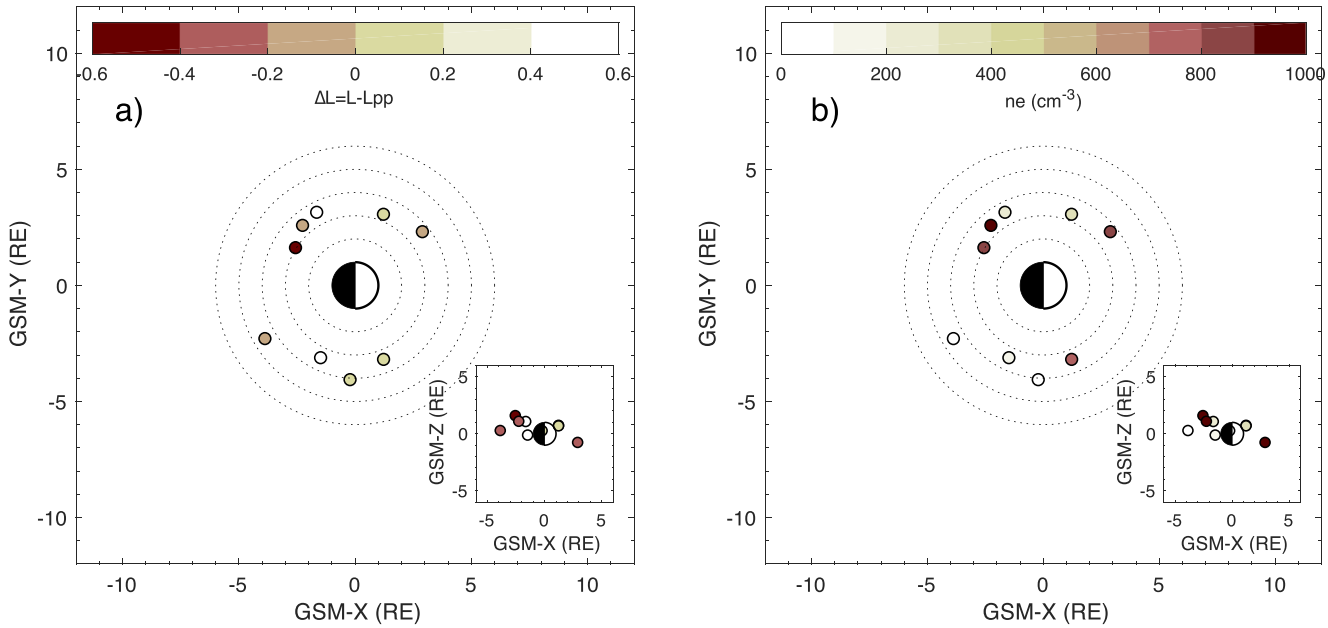

Figure 7. Initial enhancement events in the GSM coordinates. The colors in (a and b) represent the distance between the inner boundary of initial enhancement events and the simulated innermost L_{pp} (ΔL) and the corresponding plasma density, respectively.

three out of 231 initial enhancement events were found inside of the simulated innermost L_{pp}. As detailed in Goldstein, Pascuale, et al. (2014), the PTP simulation is generally in agreement with the Van Allen Probes' observations but there still exist discrepancies between the model and the observations especially during the quiet or weakly disturbed conditions. Our investigation of these outlier events suggests that even for those that are inside the innermost L_{pp}, they are still within the range of the model uncertainty (0.40 ± 0.05).

The colors in Figure 7b, on the other hand, represent the corresponding plasma density at the inner boundary of initial enhancement events. A plasma density less than 100 cm^{-3} suggests that the spacecraft is outside of the in situ L_{pp} and vice versa. We note that the "outlier" initial enhancement events near the post-midnight sector are found outside the in situ L_{pp}, while those near the duskside are inside the in situ L_{pp}. The MLT of the innermost L_{pp} in Table 1 also indicates that the innermost L_{pp} for these nine events were identified near the post-midnight and pre-noon sectors between 2.5 and 8.6. These observations are consistent with the common understanding of the local-time-dependent plasmapause positions. The plasmapause near the post-midnight and pre-noon sector is generally the most earthward especially during the geomagnetic active period, while the plasmapause near the dusk side is often further away from the Earth. The observed initial enhancements near duskside thus are more likely to be found inside the in situ L_{pp} than those near the midnight sectors, as shown in Table 1 and Figure 7b. Therefore, it warrants caution when using the location of the enhancements with respect to the in situ L_{pp} to infer the effect of convective electric field on the energetic electrons.

4. Phase Space Density Analysis

The in situ nature of the spacecraft measurements and the uncertainty associated with the plasmapause simulation make it hard to fully capture the relationship between the plasmapause locations and these outlier enhancement events. To further investigate these outlier events, we conduct a phase space density analysis. The idea behind this is that if it is the large-scale electric field that transports energetic electrons inward and erodes the plasmasphere, we will likely observe an inward shift of the phase space density gradient, rather than a local peak in the phase space density. We converted flux to phase space density as a function of the three adiabatic invariants, μ, K, and L^*, and examined the phase space density profile during the enhancement events (dashed lines in Figures 8 and 9) as well as the closest prior pass (solid lines in Figures 8 and 9) for both the October 14, 2014 event and the July 25, 2013 event.

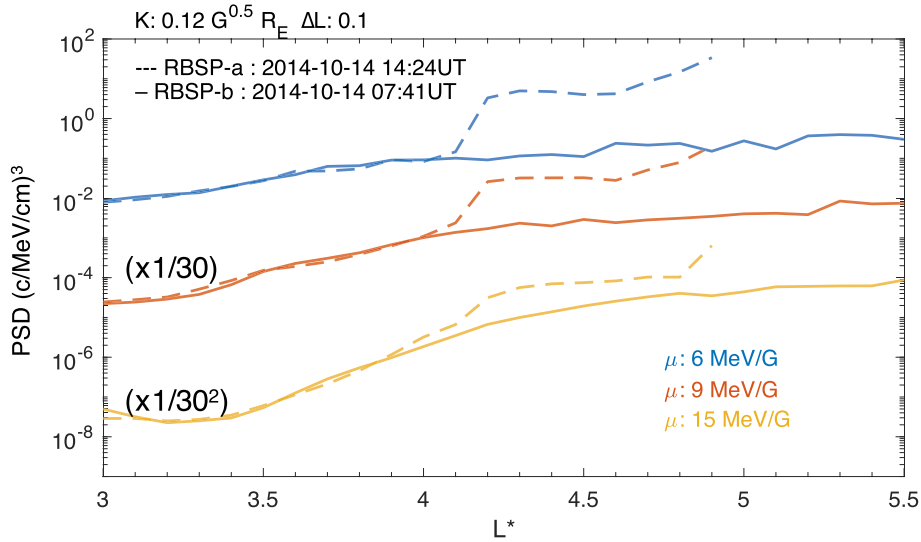

Figure 8. Phase space density evolution between two successive outbound passes by Van Allen Probes on October 14, 2014 at three μ values of 6, 9, 15 MeV/G, and K of 0.12 $G^{0.5}R_E$. The time on the top left indicates the time when the RBSP-A/B passed $L^* = 4$ during their corresponding outbound pass.

The phase space density evolution between the outbound pass where the initial enhancement of 32 keV electrons was identified by RBSP-A and the prior outbound pass observed by RBSP-B during the October 14, 2014 event is presented in Figure 8. We selected μ values of 6, 9, and 15 MeV/G for this event, which translates to 73 keV, 117 keV, and 151 keV at $L^* = 4$ during this storm period. For this event, we choose $K = 0.12\ G^{0.5}R_E$, which corresponds to electrons with equatorial pitch angles of 38°–52° for $L^* = 3$–5.5. RBSP-B passed $L^* = 4$ at 07:41 UT during its outbound pass, and in the subsequent outbound pass where the initial enhancement event was observed, RBSP-A passed $L^* = 4$ at 14:24 UT. Due to the orbit of the spacecraft and the variations in the geomagnetic latitude that they cover, the prior outbound pass observed a wider range of L and L^*, as shown in Figures 1d and 8. The relatively weak geomagnetic activity a few weeks before the event could explain the rather flat phase space density profile we observed at the pass before the initial enhancements (the solid line in Figure 8). With the lack of local peaks in the phase space density

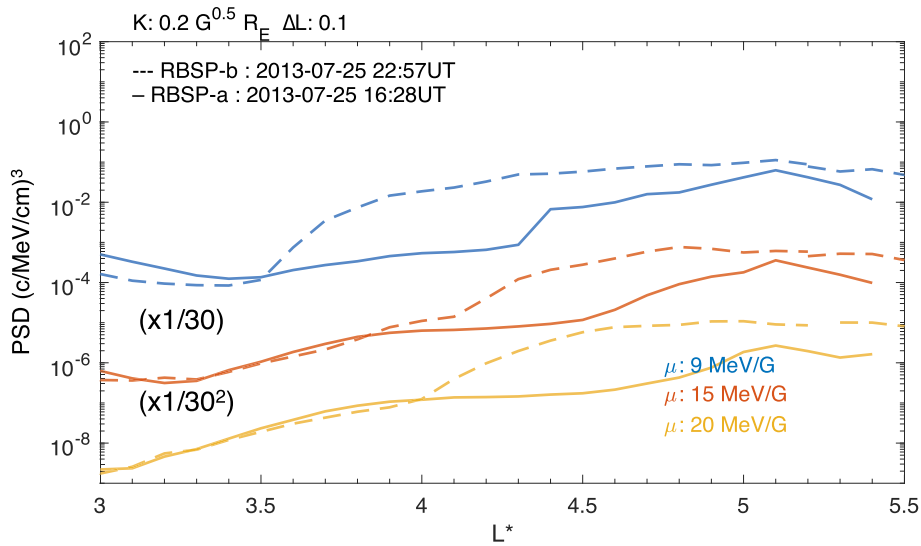

Figure 9. Phase space density evolution between two successive outbound passes by Van Allen Probes on July 25, 2013 at three μ values of 9, 15, 20 MeV/G and K of 0.2 $G^{0.5}R_E$. The time on the top left indicates the time when the RBSP-A/B passed $L^* = 4$ during their corresponding outbound pass.

profile during the initial enhancement pass, radial transport of electrons is favored as the underlying mechanism for this initial enhancement event.

To study the initial sudden enhancements of <145 keV electrons during the July 25, 2013 event, we look at three distinct μ values: 9, 15, and 20 MeV/G, which translates to 38, 57, and 92 keV at $L^* = 4$, respectively. We choose $K = 0.2$ $G^{0.5}R_E$, which corresponds to electrons with equatorial pitch angles of 30°–45° for $L^* = 3$–5.5 to provide sufficient statistics for this analysis. From Figure 9, it is clear that the radial gradient of the PSD moves radially inward between two consecutive outbound passes. This suggests that the flux enhancement described in Section 3.2 is also likely due to inward radial transport. The same type of phase space density evolution was observed by Califf et al. (2017). Using a simple large-scale convection electric field model, they successfully reproduced a similar PSD evolution. Their study emphasizes the importance of time-varying electric fields to produce a net inward radial transport of energetic electrons. It is noted that the time-varying enhanced electric field is also responsible for the erosion of the main plasmasphere and the formation of the plasmaspheric bulge and/or plume near the duskside. This is in agreement with our observations in Section 3.2 that the inner boundary of the initial enhancement near duskside is outside of the simulated innermost L_{pp} but inside the in situ L_{pp}. In short, the phase space density analysis for these two events points to inward radial transport as the underlying mechanism for the initial sudden flux enhancements. This is pertinent to the effect of enhanced electric field on the energetic electrons and the plasmasphere, and it is consistent with our findings in Section 3.

5. Discussion and Conclusion

This study examined multiple events where enhancements were previously reported inside the in situ L_{pp} or the simulated innermost L_{pp}. A close inspection of these nine "outlier" events reveals a local-time dependency of the relationship between the observed initial enhancements and the in situ L_{pp} that is inferred using the density threshold of $n_e = 100$ cm^{-3}. In this study, two out of the three initial enhancement events detected near the postmidnight sector are found outside the in situ L_{pp}. In the meantime, the initial sudden enhancement events detected near noon/dusk sectors are found inside the in situ L_{pp} but remain outside of the innermost L_{pp} (within the plasmapause uncertainty), as demonstrated in six out of nine outlier events that we studied here (see Table 1 and Figure 7). The satellite observations are limited by their localized nature and hence lack the global contextual information of the plasma population. Meanwhile, the inner magnetosphere dynamic is temporal and local time-dependent. The distinction between the in situ L_{pp} and the innermost L_{pp} is thus an important one to make.

After taking uncertainties of the plasmapause model into accounts, our study suggests that the innermost L_{pp} remains the innermost limit for the initial sudden enhancements of energetic electrons. This correlation has been observed by previous studies (Khoo et al., 2018, 2019; Li et al., 2006), and this study shows that this relation persists even in events that were previously regarded as "outliers". Thaller et al. (2015) have demonstrated a clear coincidence between the electric field enhancement and the plasmaspheric erosion using Van Allen Probes data. Note that plasmasphere dynamics are subjected to both convection electric field and SAPS (Goldstein et al., 2003), as were the PTP simulations used in this study. Our findings thus suggest that the large-scale duskward electric field that is responsible for the plasmaspheric erosion can also transport the energetic electrons to low L-shells. These large-scale electric fields could be a result of enhanced global convection and/or localized electric field structure like SAPS (Goldstein et al., 2003). It is thus important to note that our findings bespeak the role of the large-scale electric fields in these sudden enhancement events without isolating the source of these fields.

In summary, we have shown that due to the localized nature of satellite measurements and the spatio-temporal dependency of the inner magnetosphere dynamics, the initial sudden enhancement locations are more commonly found inside the in situ L_{pp} when the observations were made near the noon/dusk sectors where the local L_{pp} is usually at a larger L value. Unlike the comparison of the measured enhanced energetic electrons with the in situ L_{pp}, our study suggests that the innermost L_{pp} presents the limit of the inner boundary of the initial enhancements of energetic electrons regardless. The phase space density analysis further implies that inward radial transport is responsible for these initial enhancement events. These observations fit the understanding of the role of large-scale electric fields on energetic electrons and

the plasmasphere. This study also inherently implores cautions when using the comparison between the measured particle enhancement locations and the in situ L_{pp} to imply the effect of large-scale electric fields on energetic electrons. Finally, insights from this study will allow us to leverage advances in the modeling of plasmapause/plasma density to infer the initial enhancement location of energetic electrons and improve predictive simulations of energetic electron dynamics.

Data Availability Statement

All Van Allen Probes ECT/MagEIS data, the spacecraft magnetic ephemeris data, and the PTP plasmapause simulation outputs are publicly available at www.rbsp-ect.lanl.gov. The solar parameters and geomagnetic indices used in this study are obtained from the OMNI database (http://omniweb.gsfc.nasa.gov). Data from GOES spacecraft is obtained from https://cdaweb.gsfc.nasa.gov/pub/data/goes/. The plasma density results derived from EMFISIS and EFW instrument onboard Van Allen probes are publicly available at https://cdaweb.gsfc.nasa.gov/pub/data/rbsp as well as http://www.space.umn.edu/rbspefw-data/.

Acknowledgments
The authors would like to thank Theodore Sarris for helpful discussions and constructive feedback on the draft manuscript. This work was supported in part by NASA grant NSSC19K0237 and 80NSSC18K1119, and by NASA/RBSP-ECT funding through JHU/APL contract 967399 under prime NASA contract NAS5-01072. H. Zhao was supported by NASA Grant 80NSSC20K0694.

References

Blake, J. B., Carranza, P. A., Claudepierre, S. G., Clemmons, J. H., Crain, W. R., Dotan, Y., et al. (2013). *The Magnetic Electron Ion Spectrometer (MagEIS) instruments aboard the Radiation Belt Storm Probes (RBSP) spacecraft* (pp. 383–421). The Van Allen Probes Mission. https://doi.org/10.1007/978-1-4899-7433-4_12

Burch, J. L., Goldstein, J., & Sandel, B. R. (2004). Cause of plasmasphere corotation lag. *Geophysical Research Letters*, *31*, L05802. https://doi.org/10.1029/2003GL019164

Califf, S., Li, X., Wolf, R. A., Zhao, H., Jaynes, A. N., Wilder, F. D., et al. (2016). Large-amplitude electric fields in the inner magnetosphere: Van Allen Probes observations of subauroral polarization streams. *Journal of Geophysical Research: Space Physics*, *121*, 5294–5306. https://doi.org/10.1002/2015JA022252

Califf, S., Li, X., Zhao, H., Kellerman, A., Sarris, T. E., Jaynes, A., & Malaspina, D. M. (2017). The role of the convection electric field in filling the slot region between the inner and outer radiation belts. *Journal of Geophysical Research: Space Physics*, *122*, 2051–2068. https://doi.org/10.1002/2016JA023657

Carpenter, D. L., & Anderson, R. R. (1992). An ISEE/whistler model of equatorial electron density in the magnetosphere. *Journal of Geophysical Research*, *97*(A2), 1097–1108. https://doi.org/10.1029/91JA01548

Chappell, C. R., Harris, K. K., & Sharp, G. W. (1970). A study of the influence of magnetic activity on the location of the plasmapause as measured by OGO 5. *Journal of Geophysical Research*, *75*(1), 50–56. https://doi.org/10.1029/JA075i001p00050

Chen, Y., Friedel, R. H. W., & Reeves, G. D. (2006). Phase space density distributions of energetic electrons in the outer radiation belt during two Geospace Environment Modeling Inner Magnetosphere/Storms selected storms. *Journal of Geophysical Research*, *111*(A11).

Escoubet, C. P., Pedersen, A., Schmidt, R., & Lindqvist, P. A. (1997). Density in the magnetosphere inferred from ISEE 1 spacecraft potential. *Journal of Geophysical Research*, *102*(A8), 17595–17609. https://doi.org/10.1029/97JA00290

Finlay, C. C., Maus, S., Beggan, C. D., Bondar, T. N., Chambodut, A., Chernova, T. A., et al. (2010). International geomagnetic reference field: The eleventh generation. *Geophysical Journal International*, *183*, 1216–1230. https://doi.org/10.1111/j.1365-246X.2010.04804.x

Foster, J. C., Erickson, P. J., Baker, D. N., Claudepierre, S. G., Kletzing, C. A., Kurth, W., et al. (2014). Prompt energization of relativistic and highly relativistic electrons during a substorm interval: Van Allen Probes observations. *Geophysical Research Letters*, *41*, 20–25. https://doi.org/10.1002/2013GL058438

Frank, L. A. (1971). Relationship of the plasma sheet, ring current, trapping boundary, and plasmapause near the magnetic equator and local midnight. *Journal of Geophysical Research*, *76*(10), 2265–2275. https://doi.org/10.1029/JA076i010p02265

Goldstein, J., Baker, D. N., Blake, J. B., De Pascuale, S., Funsten, H. O., Jaynes, A. N., et al. (2016). The relationship between the plasmapause and outer belt electrons. *Journal of Geophysical Research: Space Physics*, *121*, 8392–8416. https://doi.org/10.1002/2016JA023046

Goldstein, J., Kanekal, S., Baker, D. N., & Sandel, B. R. (2005). Dynamic relationship between the outer radiation belt and the plasmapause during March–May 2001. *Geophysical Research Letters*, *32*, L15104. https://doi.org/10.1029/2005GL023431

Goldstein, J., Pascuale, S. D., Kletzing, C., Kurth, W., Genestreti, K. J., Skoug, R. M., et al. (2014). Simulation of Van Allen Probes plasmapause encounters. *Journal of Geophysical Research: Space Physics*, *119*, 7464–7484. https://doi.org/10.1002/2014JA020252

Goldstein, J., Sandel, B. R., Forrester, W. T., Thomsen, M. F., & Hairston, M. R. (2005). Global plasmasphere evolution April 22–23, 2001. *Journal of Geophysical Research*, *110*, A12218. https://doi.org/10.1029/2005JA011282

Goldstein, J., Sandel, B. R., Hairston, M. R., & Reiff, P. H. (2003). Control of plasmaspheric dynamics by both convection and sub-auroral polarization stream. *Geophysical Research Letters*, *30*, 224324. https://doi.org/10.1029/2003GL018390

Goldstein, J., Thomsen, M. F., & DeJong, A. (2014). In situ signatures of residual plasmaspheric plumes: Observations and simulation. *Journal of Geophysical Research: Space Physics*, *119*, 4706–4722. https://doi.org/10.1002/2014JA019953

Hanser, F. A. (2011). *EPS/HEPAD calibration and data handbook, Tech. Rep. GOESN- ENG-048D, Assurance Technology Corporation, Carlisle, Mass.* Retrieved from http://www.ngdc.noaa.gov/stp/satellite/goes/documentation.html

Hudson, M., Kotelnikov, A., Li, X., Roth, I., Temerin, M., Wygant, J., & Gussenhoven, M. (1995). Simulation of proton radiation belt formation during the March 24, 1991 SSC. *Geophysical Research Letters*, *22*(3), 291–294. https://doi.org/10.1029/95gl00009

Jahn, J.-M., Goldstein, J., Kurth, W. S., Thaller, S., De Pascuale, S., Wygant, J., et al. (2020). Determining plasmaspheric density from the upper hybrid resonance and from the spacecraft potential: How do they compare? *Journal of Geophysical Research: Space Physics*, *125*, e2019JA026860. https://doi.org/10.1029/2019ja026860

Khoo, L.-Y., Li, X., Zhao, H., Chu, X., Xiang, Z., & Zhang, K. (2019). How sudden, intense energetic electron enhancements correlate with the innermost plasmapause locations under various solar wind drivers and geomagnetic conditions. *Journal of Geophysical Research: Space Physics*, *124*, 8992–9002. https://doi.org/10.1029/2019ja027412

Khoo, L. Y., Li, X., Zhao, H., Sarris, T. E., Xiang, Z., Zhang, K., et al. (2018). On the initial enhancement of energetic electrons and the innermost plasmapause locations: Coronal mass ejection-driven storm periods. *Journal of Geophysical Research: Space Physics*, *123*, 9252–9264. https://doi.org/10.1029/2018ja026074

Kivelson, M. G., & Russell, C. T. (Eds.) (1995). *Introduction to space physics*. Cambridge university press.

Kletzing, C. A., Kurth, W. S., Acuna, M., MacDowall, R. J., Torbert, R. B., Averkamp, T., et al. (2013). The Electric and Magnetic Field Instrument Suite and Integrated Science (EMFISIS) on RBSP. *Space Science Reviews*, *179*, 127–181. https://doi.org/10.1007/s11214-013-9993-6

Kurth, W. S., De Pascuale, S., Faden, J. B., Kletzing, C. A., Hospodarsky, G. B., Thaller, S., & Wygant, J. R. (2015). Electron densities inferred from plasma wave spectra obtained by the Waves instrument on Van Allen Probes. *Journal of Geophysical Research: Space Physics*, *120*, 904–914. https://doi.org/10.1002/2014JA020857

Lejosne, S., Kunduri, B. S. R., Mozer, F. S., & Turner, D. L. (2018). Energetic electron injections deep into the inner magnetosphere: A result of the subauroral polarization stream (SAPS) potential drop. *Geophysical Research Letters*, *45*, 3811–3819. https://doi.org/10.1029/2018gl077969

Lemaire, J. F., & Gringauz, K. .I. (1998). *The Earth's plasmasphere*. Cambridge Univ .Press.

Li, X., Baker, D. N., O'Brien, T. P., Xie, L., & Zong, Q. G. (2006). Correlation between the inner edge of outer radiation belt electrons and the innermost plasmapause location. *Geophysical Research Letters*, *33*, L14107. https://doi.org/10.1029/2006GL026294

Li, X., Roth, I., Temerin, M., Wygant, J., Hudson, M. K., & Blake, J. B. (1993). Simulation of the prompt energization and transport of radiation particles during the March 23, 1991 SSC. *Geophysical Research Letters*, *20*, 2423. https://doi.org/10.1029/93GL02701

Liu, S., Chen, M. W., Lyons, L. R., Korth, H., Albert, J. M., Roeder, J. L., et al. (2003). Contribution of convective transport to storm time ring current electron injection. *Journal of Geophysical Research*, *108*, 1372. https://doi.org/10.1029/2003JA010004

Liu, X., Liu, W., Cao, J. B., Fu, H. S., Yu, J., & Li, X. (2015). Dynamic plasmapause model based on THEMIS measurements. *Journal of Geophysical Research: Space Physics*, *120*(10), 10543–10556. https://doi.org/10.1002/2015JA021801

Malaspina, D. M., Jaynes, A. N., Boulé, C., Bortnik, J., Thaller, S. A., Ergun, R. E., et al. (2016). The distribution of plasmaspheric hiss wave power with respect to plasmapause location. *Geophysical Research Letters*, *43*, 7878–7886. https://doi.org/10.1002/2016GL069982

Mauk, B. H., Fox, N. J., Kanekal, S. G., Kessel, R. L., Sibeck, D. G., & Ukhorskiy, A. A. (2013). Science objectives and rationale for the Radiation Belt Storm Probes mission. *Space Science Reviews*, *179*(1–4), 3–27. https://doi.org/10.1007/s11214-012-9908-y

Moldwin, M. B., Downward, L., Rassoul, H. K., Amin, R., & Anderson, R. R. (2002). A new model of the location of the plasmapause: CRRES results. *Journal of Geophysical Research*, *107*(A11), 1339. https://doi.org/10.1029/2001JA009211

Ni, B., Huang, H., Zhang, W., Gu, X., Zhao, H., Li, X., et al. (2019). Parametric sensitivity of the formation of reversed electron energy spectrum caused by plasmaspheric hiss. *Geophysical Research Letters*, *46*, 4134–4143. https://doi.org/10.1029/2019gl082032

Olson, W. P., & Pfitzer, K. A. (1977). *Magnetospheric magnetic field modeling, Ann. Sci. Rep. F44620-75-C-0033*. Air Force Off. of Sci. Res.

Reeves, G. D., Friedel, R. H. W., Larsen, B. A., Skoug, R. M., Funsten, H. O., Claudepierre, S. G., et al. (2016). Energy-dependent dynamics of keV to MeV electrons in the inner zone, outer zone, and slot regions. *Journal of Geophysical Research: Space Physics*, *121*, 397–412. https://doi.org/10.1002/2015JA021569

Roederer, J. G. (1970). *Dynamics of magnetically trapped particles*. Springer.

Schiller, Q., Kanekal, S. G., Jian, L. K., Li, X., Jones, A., Baker, D. N., et al. (2016). Prompt injections of highly relativistic electrons induced by interplanetary shocks: A statistical study of Van Allen Probes observations. *Geophysical Research Letters*, *43*(24), 12317–12324. https://doi.org/10.1002/2016GL071628

Sergeev, V. A., Shukhtina, M. A., Rasinkangas, R., Korth, A., Reeves, G. D., Singer, H. J., et al. (1998). Event study of deep energetic particle injections during substorm. *Journal of Geophysical Research*, *103*(A5), 9217–9234. https://doi.org/10.1029/97JA03686

Shen, X.-C., Hudson, M. K., Jaynes, A., Shi, Q., Tian, A., Claudepierre, S., et al. (2017). Statistical study of the storm time radiation belt evolution during Van Allen Probes era: CME- vs. CIR-driven storms. *Journal of Geophysical Research: Space Physics*, *122*, 8327–8339. https://doi.org/10.1002/2017JA024100

Stern, D. P. (1975). The motion of a proton in the equatorial magnetosphere. *Journal of Geophysical Research*, *80*, 595–599. https://doi.org/10.1029/JA080i004p00595

Su, Y.-J., Selesnick, R. S., & Blake, J. B. (2016). Formation of the inner electron radiation belt by enhanced large-scale electric fields. *Journal of Geophysical Research: Space Physics*, *121*, 8508–8522. https://doi.org/10.1002/2016JA022881

Thaller, S. A., Wygant, J. R., Cattell, C. A., Breneman, A. W., Tyler, E., Tian, S., et al. (2019). Solar rotation period driven modulations of plasmaspheric density and convective electric field in the inner magnetosphere. *Journal of Geophysical Research: Space Physics*, *124*, 1726–1737. https://doi.org/10.1029/2018ja026365

Thaller, S. A., Wygant, J. R., Dai, L., Breneman, A. W., Kersten, K., Cattell, C. A., et al. (2015). Van Allen Probes investigation of the large-scale duskward electric field and its role in ring current formation and plasmasphere erosion in the June 1, 2013 storm. *Journal of Geophysical Research: Space Physics*, *120*, 4531–4543. https://doi.org/10.1002/2014JA020875

Thorne, R. M. (2010). Radiation belt dynamics: The importance of wave-particle interactions. *Geophysical Research Letters*, *37*, L22107. https://doi.org/10.1029/2010GL044990

Tsyganenko, N. A. (1989). A magnetospheric magnetic field model with a warped tail current sheet. *Planetary and Space Science*, *37*, 5–20. https://doi.org/10.1016/0032-0633(89)90066-4

Tsyganenko, N. A., & Sitnov, M. I. (2005). Modeling the dynamics of the inner magnetosphere during strong geomagnetic storms. *Journal of Geophysical Research*, *110*, A03208. https://doi.org/10.1029/2004JA010798

Turner, D. L., Claudepierre, S. G., Fennell, J. F., O'Brien, T. P., Blake, J. B., Lemon, C., et al. (2015). Energetic electron injections deep into the inner magnetosphere associated with substorm activity. *Geophysical Research Letters*, *42*, 2079–2087. https://doi.org/10.1002/2015GL063225

Turner, D. L., O'Brien, T. P., Fennell, J. F., Claudepierre, S. G., Blake, J. B., Jaynes, A. N., et al. (2017). Investigating the source of near-relativistic and relativistic electrons in Earth's inner radiation belt. *Journal of Geophysical Research: Space Physics*, *122*, 695–710. https://doi.org/10.1002/2016JA023600

Volland, H. (1973). A semiempirical model of large-scale magnetospheric electric fields. *Journal of Geophysical Research*, *78*, 171–180. https://doi.org/10.1029/JA078i001p00171

Wang, D., Shprits, Y. Y., Zhelavskaya, I. S., Effenberger, F., Castillo, A., Drozdov, A. Y., et al. (2020). The effect of plasma boundaries on the dynamic evolution of relativistic radiation belt electrons. *Journal of Geophysical Research: Space Physics*, *125*, e2019JA027422. https://doi.org/10.1029/2019ja027422

Wygant, J. R., Bonnell, J. W., Goetz, K., Ergun, R. E., Mozer, F. S., Bale, S. D., et al. (2013). The electric field and waves instruments on the Radiation Belt Storm Probes Mission. *Space Science Reviews*, *179*, 183–220. https://doi.org/10.1007/s11214-013-0013-7

Zhao, H., Baker, D. N., Califf, S., Li, X., Jaynes, A. N., Leonard, T., & Spence, H. E. (2017). Van Allen probes measurements of energetic particle deep penetration into the low L region ($L < 4$) during the storm on April 8, 2016. *Journal of Geophysical Research: Space Physics*, *122*(12), 12140–12152. https://doi.org/10.1002/2017ja024558

Zhao, H., Ni, B., Li, X., Baker, D. N., Johnston, W. R., Zhang, W., et al. (2019). Plasmaspheric hiss waves generate a reversed energy spectrum of radiation belt electrons. *Nature Physics*, *15*, 367–372. https://doi.org/10.1038/s41567-018-0391-6